Electronic Supplementary Material (ESI) for Materials Chemistry Frontiers.

Electronic Supplementary Information

for

Ionic electroactive PEDOT:PSS/liquid-crystalline polymer electrolyte actuators: Photopolymerization of zwitterionic columnar liquid crystals complexed with a protic ionic liquid

Siyu Cao, Chengyang Liu, and Masafumi Yoshio*

Molecular Mechatronics Group, Research Center for Macromolecules & Biomaterials, National Institute for Materials Science, Tsukuba, Ibaraki 305-0047, Japan; Graduate School of Chemical Sciences and Engineering, Hokkaido University, Sapporo, Hokkaido 060-8628, Japan

*E-mail: YOSHIO.Masafumi@nims.go.jp

1. Characterization of liquid crystallinity

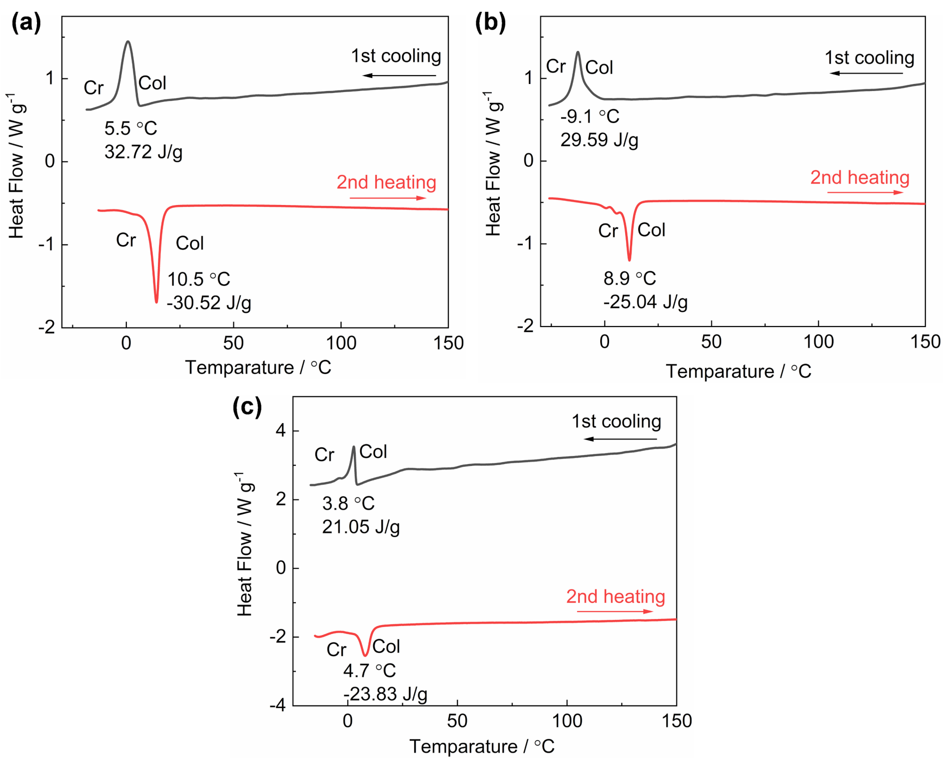

Fig. S1 DSC thermograms of (a) **M1/2(40)**, (b) **M1/2(50)**, and (c) **M1/2(60)**. The transition temperatures were taken at the peak tops.

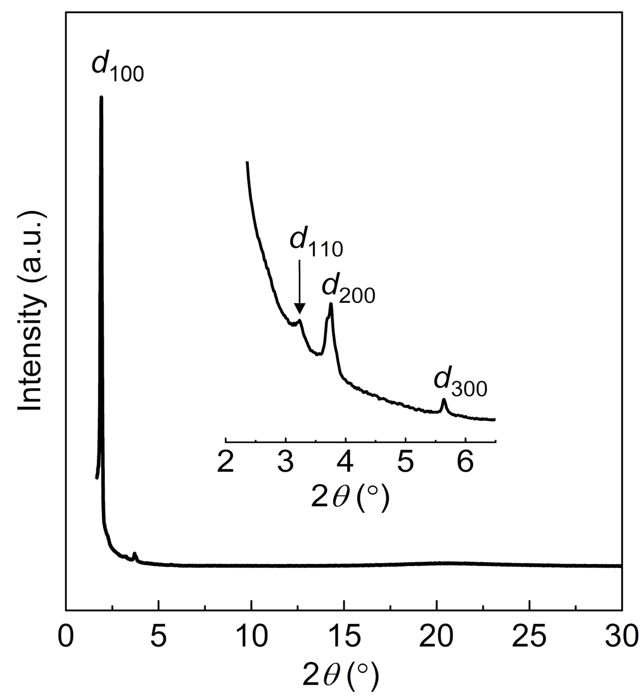

Fig. S2 XRD pattern of **M1/2(50)** at room temperature.

The number of molecules (n) per cross-sectional slice of the column for **M1/2(50)** was estimated as 10 using the equation $n = (\sqrt{3}N_A a^2 h\rho)/2M$, where N_A is Avogadro's number (6.02×10^{23} mol^{-1}), ρ is density, M is molecular weight, and h is the average height of the stratum; h was estimated as 4.4 Å from the position of a halo at $2\theta = 20°$. ρ was estimated as 1.0 g cm^{-3}.

2. *In situ* photopolymerization of the LC mixtures

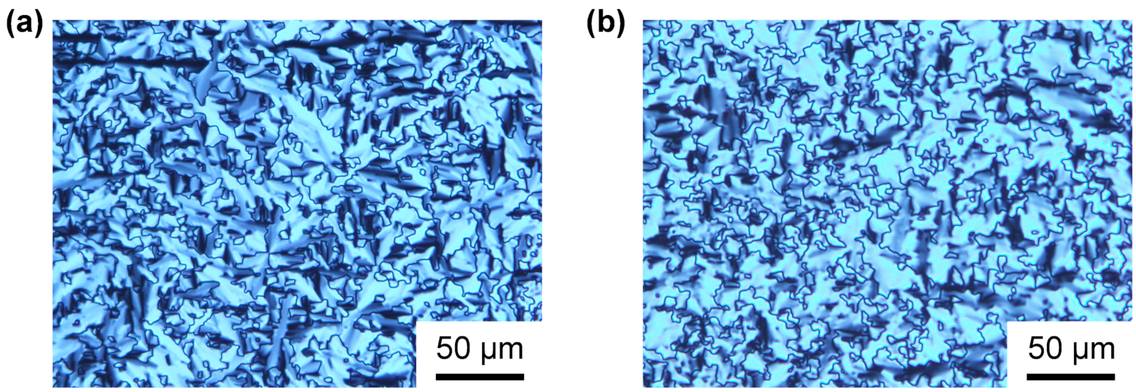

Fig. S3 Polarizing optical micrographs at room temperature: (a) **M1/2(50)** and (b) **P1/2(50)**.

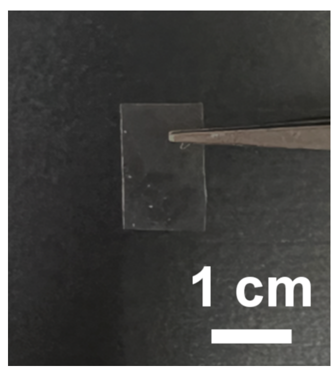

Fig. S4 Photograph of a free-standing polymer film of **P1/2(50)**.

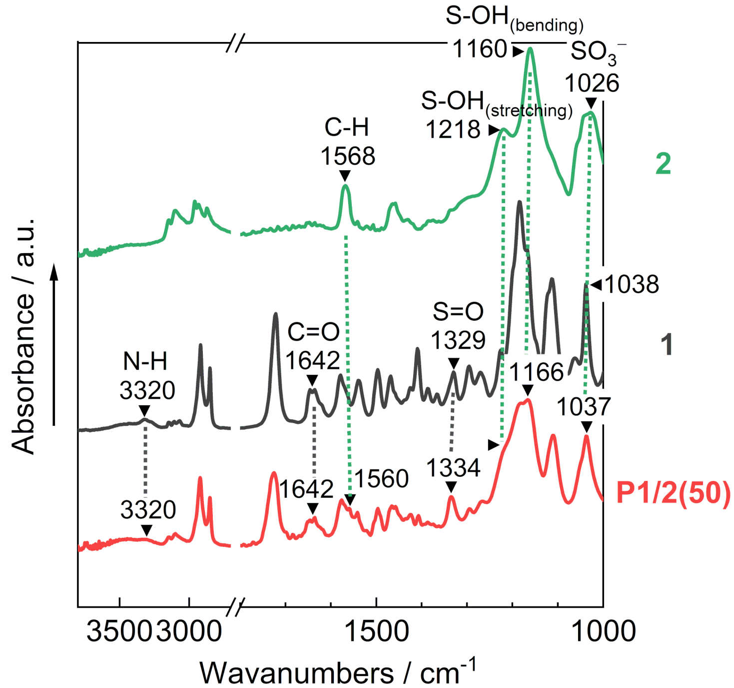

Fig. S5 FT-IR spectra of **2** (green line), **1** (black line), and **P1/2 (50)** (red line) at room temperature.

3. Ionic Conductivity

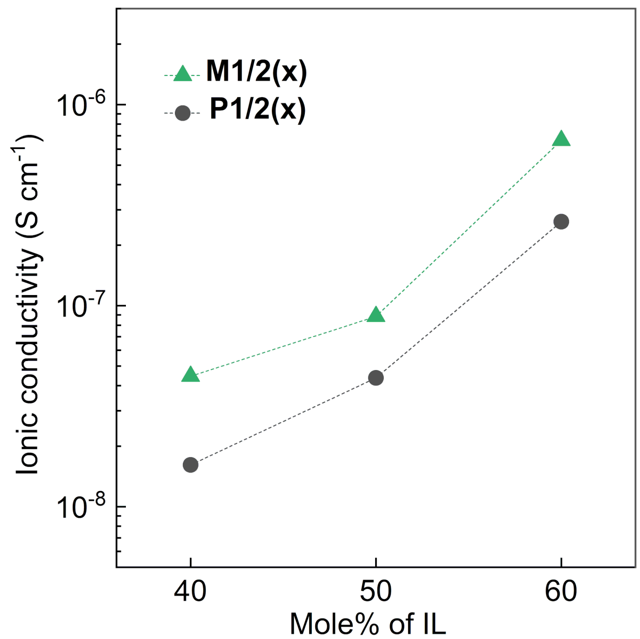

Fig. S6 Ionic conductivities of **M1/2(x)** and polymer films **P1/2(x)** at room temperature.

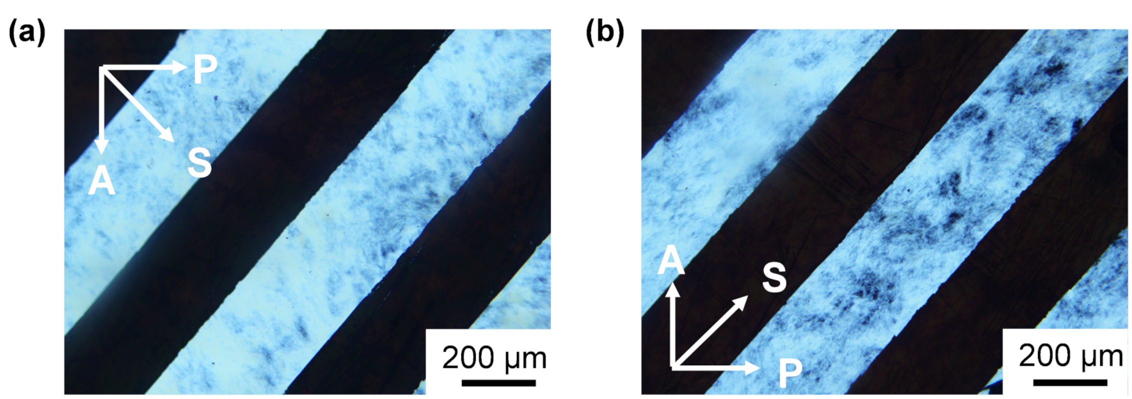

Fig. S7 POM images of aligned **M1/2(50)** between comb-shaped gold electrodes at ambient conditions: (a) perpendicular orientation of the columnar axis to the direction of electrodes (⊥); (b) parallel orientation of the columnar axis to the direction of electrodes (//).

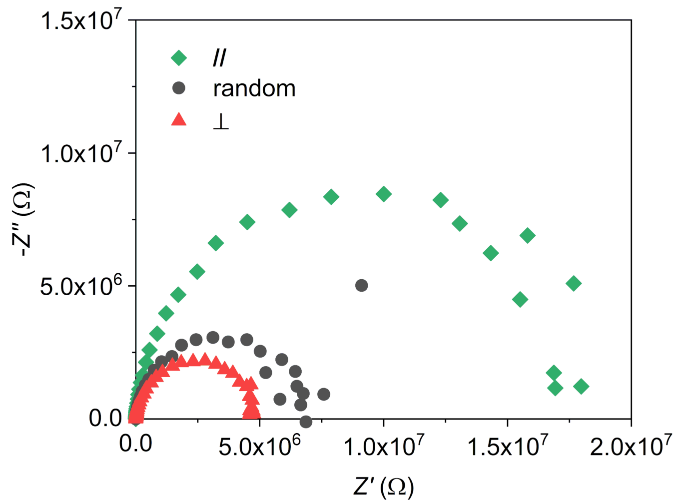

Fig. S8 Nyquist plots of **M1/2(50)** with random orientation and uniaxially planar orientation of columns between comb-shaped gold electrodes at ambient conditions. // and ⊥ indicates that the columnar axis is parallel and perpendicular to the direction of gold electrodes, respectively.

4. Actuation Performance

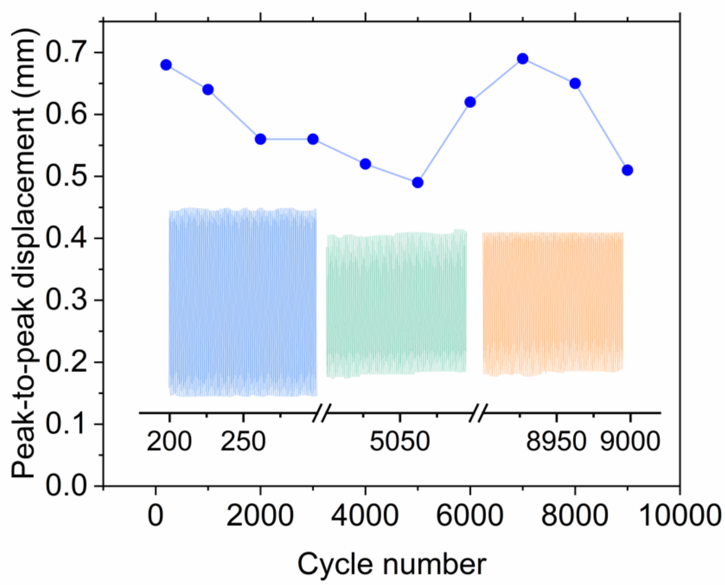

Fig. S9 Cycle stability of the bending actuation for the **P1/2(50)**-based actuator under 2 V at 1 Hz.

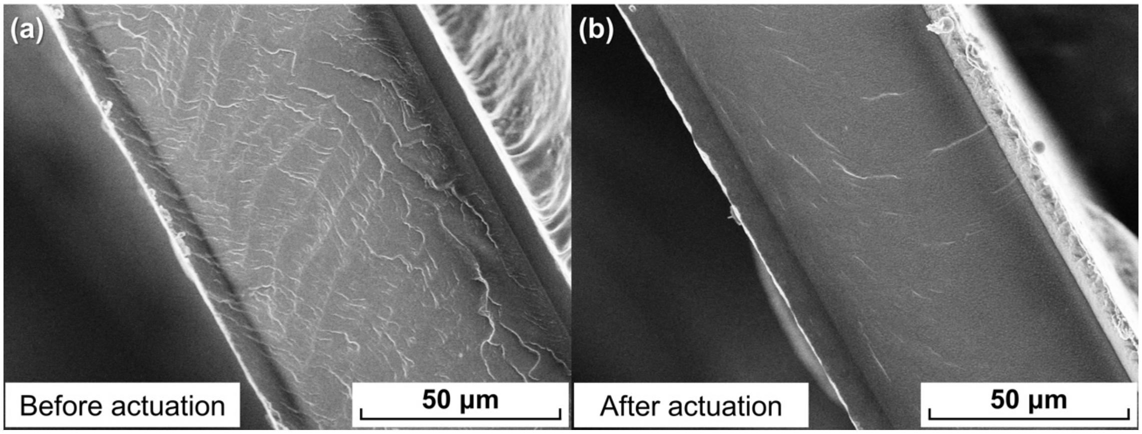

Fig. S10 SEM images of the cross-section of the **P1/2(50)**-based actuator before and after long-term actuation experiment.

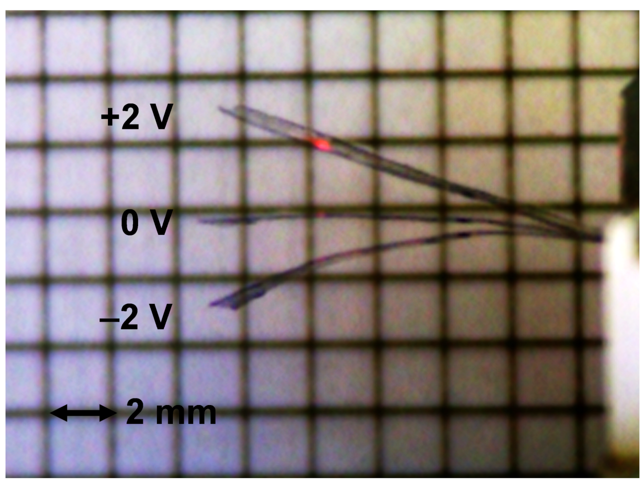

Fig. S11 Photograph of the **P1/2(50)-**based actuator under an AC voltage of 2 V at 0.1 Hz. The thickness of actuator is 68 μm.

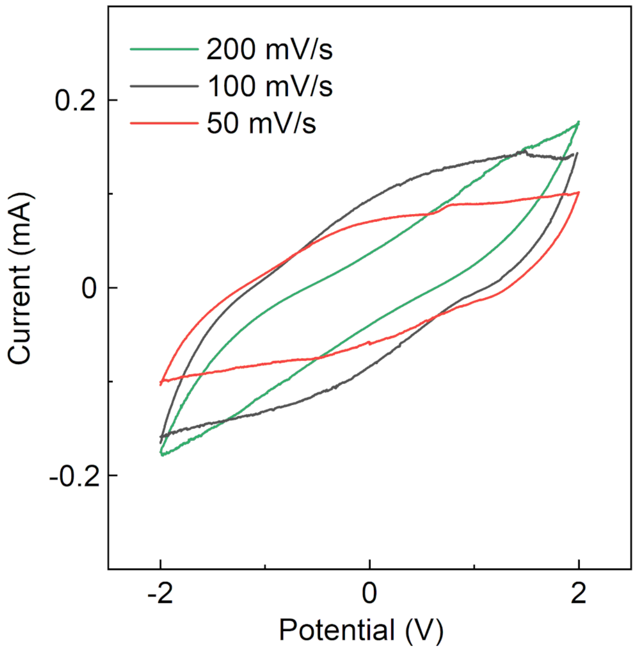

Fig. S12 Cyclic voltammograms of the **P1/2(50)** actuator under a potential window between +2 and –2 V at scan rates of 200, 100, and 50 mV s^{-1} under ambient condition. The electrolyte thickness of **P1/2(50)** is 57 µm.

Table S1. Summary of bending strains and blocking forces between different actuators.

Electrolyte	Electrode	IL (wt%)	V_{AC} (V)	Frequency (Hz)	Bending strain (%)	V_{DC} (V)	Blocking force (mN)	Normalized force[a] (kPa)
This work		$[BMIM]^+[HSO_4]^-$						
75-μm-thick P1/2(60)	PEDOT:PSS	24.8 wt%	2	0.1	0.67	2	4.68	1170
75-μm-thick P1/2(50)	PEDOT:PSS	18.1 wt%	2	0.01	0.86	1	1.45	337
75-μm-thick P1/2(40)	PEDOT:PSS	12.8 wt%	2	0.01	0.59	1	1.24	372
1D columnar LC membrane [S1]	PEDOT:PSS	$[EMIM]^+[BF_4]^-$ 7.9 wt%	2	0.01	0.20	2	0.27	392
3D columnar LC membrane [S2]	PEDOT:PSS	$[EMIM]^+[BF_4]^-$ 5.6 wt%	2	0.01	0.81	2	1.10	204
3D LC/polymer composite membrane [S3]	PEDOT:PSS	$[BMIM]^+[CF_3SO_3]^-$ 27.5 wt%	1	0.1	0.32	2	0.27	42
PVDF [S4]	Ni-CAT NWAs/CNF	$[EMIM]^+[TFSI]^-$ 60 wt%	3	0.1	0.36	3[b]	1.45	1510
Cellulose [S5]	PEDOT:PSS	$[EMIM]^+[BF_4]^-$ 70 wt%	2	0.1	0.28	2	1.01	606
Block copolymer (PSS-b-PMB) [S6]	P(VdF-HFP)/SWCNTs/ $[EMIM]^+[BF_4]^-$	ZIms 50 mol%	2	0.5	0.87	1	0.3	516
Polyimide-Nafion [S7]	Pt	-	3	0.1	0.28	3	5.93	272
Nafion 117 [S7]	Pt	-	3	0.1	0.21	3	6.86	233
Sulfonated polyimide [S8]	Carbon composite	$[EMIM]^+[TFSI]^-$ 50-75 wt%	1.5	0.05	0.19	3	0.67	268
Thermoplastic polyurethane [S9]	PEDOT:PSS/IL/DMSO	$[EMIM]^+[TFSI]^-$ 80 wt%	2	0.1	0.61	2[c]	0.3	101
Nafion [S10]	Molybdenum-disulfide/ Graphene-oxide	$[EMIM]^+[BF_4]^-$ 37.5 wt%	1.5	0.1	1.27	2	0.28	168
Covalent organic frameworks (COF-DT-SO3Na) [S11]	PEDOT:PSS	-	0.5	0.1	0.39	0.5[d]	1.2	1667

[a]: Normalized force ($F_{\mathrm{Nor.}}$) is calculated using the following equation [S1] $F_{\mathrm{Nor.}} = F_{\mathrm{exp.}} l/wt^2$, where $F_{\mathrm{exp.}}$ is the measuring blocking force, w, t, and l are the width, thickness, and free length of the actuator, respectively.

[b,c,d]: blocking force was measuring under applying AC voltage.

5. References

[S1] C.-H. Wu, W. Meng and M. Yoshio, Low-voltage-driven actuators using photo-cross-linked ionic columnar liquid-crystalline polymer films, *ACS Mater. Lett.*, 2022, **4**, 153–158.

[S2] C.-H. Wu, W. Meng, K. Iakoubovskii and M. Yoshio, Photocured liquid-crystalline polymer electrolytes with 3D ion transport pathways for electromechanical actuators, *ACS Appl. Mater. Interfaces*, 2023, **15**, 4495–4504.

[S3] S. Cao, J. Aimi and M. Yoshio, Electroactive soft actuators based on columnar Ionic liquid crystal/polymer composite membrane electrolytes forming 3D continuous ionic channels, *ACS Appl. Mater. Interfaces*, 2022, **14**, 43701–43710.

[S4] Y.-X. Shi, Y. Wu, S.-Q. Wang, Y.-Y. Zhao, T. Li, X.-Q. Yang and T. Zhang, Soft electrochemical actuators with a two-dimensional conductive metal–organic framework nanowire array, *J. Am. Chem. Soc.*, 2021, **143**, 4017–4023.

[S5] F. Wang, Z. Jin, S. Zheng, H. Li, S. Cho, H.J. Kim, S.-J. Kim, E. Choi, J.-O. Park and S. Park, High-fidelity bioelectronic muscular actuator based on porous carboxylate bacterial cellulose membrane, *Sens. Actuators B*, 2017, **250**, 402–411.

[S6] O. Kim, H. Kim, U.H. Choi and M.J. Park, One-volt-driven superfast polymer actuators based on single-ion conductors, *Nat. Commun.*, 2016, **7**, 13576.

[S7] J. Nam, T. Hwang, K. J. Kim and D.-C. Lee, A new high-performance ionic polymer–metal composite based on Nafion/polyimide blends, *Smart Mater. Struct.*, 2017, **26**, 035015.

[S8] S. Imaizumi, Y. Ohtsuki, T. Yasuda, H. Kokubo and M. Watanabe, Printable polymer actuators from ionic liquid, soluble polyimide, and ubiquitous carbon materials, *ACS Appl. Mater. Interfaces*, 2013, **5**, 6307–6315.

[S9] S.Y. Kim, Y. Kim, C. Cho, H. Choi, H.W. Park, D. Lee, E. Heo, S. Park, H. Lee and D.H. Kim, Deformable ionic polymer artificial mechanotransducer with an interpenetrating nanofibrillar network, *ACS Appl. Mater. Interfaces*, 2019, **11**, 29350–29359.

[S10] M.T. Manzoor, V.H. Nguyen, S. Umrao, J.H. Kim, R. Tabassian, J.E. Kim and I.K.

Oh, Mutually exclusive p-type and n-type hybrid electrode of MoS2 and graphene for artificial soft touch fingers, *Adv. Funct. Mater.*, 2019, **29**, 1905454.

[S11] F. Yu, J.-H. Ciou, S. Chen, W.C. Poh, J. Chen, J. Chen, K. Haruethai, J. Lv, D. Gao and P.S. Lee, Ionic covalent organic framework based electrolyte for fast-response ultra-low voltage electrochemical actuators, *Nat. Commun.*, 2022, **13**, 390.